Symbolic sequence statistical analysis for free liquid jets

J. Godelle and C. Letellier
CORIA UMR No. 6614, Université et INSA de Rouen, Place Emile Blondel, F-76821 Monte Saint-Aignan Cedex, France
(Received 2 December 1999; revised manuscript received 21 June 2000)

Free liquid jets are investigated here as nonlinear dynamical systems. A scalar time series corresponding to the time evolution of the jet diameter is then used to investigate the underlying dynamics in terms of reconstructed phase portraits, Poincaré sections, and first-return maps. Particular attention is paid to characterizing the behavior using symbolic sequence statistics that enable different atomization regimes to be distinguished. Such statistics are first applied on theoretical maps to support the results obtained on the jet dynamics.

PACS number(s): 47.52.+j, 05.45.−a

I. INTRODUCTION

Liquid jets have been extensively studied since the pioneering paper by Rayleigh [1]. In particular, the stability curve, i.e., the breakup length versus the fluid velocity, has been investigated by Weber [2]. More recently, it has been shown that three main classes of liquid-gas jets, i.e., a liquid jet within a gas environment, may be identified [3]. It has been observed that two of these classes may be distinguished by a perturbation growth analysis [17]. Such an analysis has been used to show that when the liquid jet dynamics is mainly governed by the internal forces due to the velocity field of the liquid flow, initial perturbations near the needle are larger than when the jet dynamics is mainly governed by the capillary instabilities. Nevertheless, jet atomization is governed by very complex dynamics that are not fully understood. Very recently, experimental studies of a forced gas-gas jet at a moderate Reynolds number have revealed that the atomization processes may be interpreted in terms of low-dimensional chaos as well as tangent bifurcations and intermittency [4]. Such features are very often observed for confined flows such as Taylor-Couette flow or Rayleigh-Bénard convection that have been studied in experiments [5–7] using tools borrowed from the theory of nonlinear dynamical systems. Nevertheless, it has been shown that such techniques may also be used for open flows, as exemplified in the works by Broze and Hussain [4]. There are other investigations of open flows where low-dimensional behaviors are observed, as in the case of the dynamics in the wake of an oscillatoring cylinder in a free stream flow [8–10] or a modulated flow through a planar symmetric channel expansion [11], among others.

Phase intermittency will be shown to be associated with atomization processes in cases where excited or free liquid-gas jets are considered. Such studies will reveal that the dynamics of liquid jets may be conveniently analyzed by using concepts introduced in the theory of nonlinear dynamical systems. In order to do that, we will investigate the nature of the dynamics by using tools such as phase portraits, first-return maps to Poincaré sections, and angular first-return maps. Symbolic sequence statistics as introduced by Tang *et al.* [12,13] will also be used. The latter approach has already been used for investigating experimental data in order to validate a model for cyclic dispersion in a car engine [14]. With the aid of these techniques, the deterministic nature of the jet dynamics will be investigated. Before an application of the symbolic sequence statistics, we will start by a study of numerical maps to explain what exactly can be learned by using such a tool. In order to do that, a few applications will be given on maps as exemplified by the logistic map or the antisymmetric cubic map.

The paper is organized as follows: In Sec. II, the experimental setup is briefly described and the dynamics of free liquid-gas jets is investigated for six different control parameter values using angular first-return maps. Section III gives a brief introduction to symbolic dynamics and how it may be used to distinguish different kinds of dynamical behavior. The six jets will then be investigated using symbolic sequence statistics. Section IV is a conclusion.

II. EXPERIMENTS

A. The experimental setup

The jet generation apparatus produces a cylindrical jet with a diameter close to the internal diameter of the injection needle, $D=600\ \mu$m. Here, the jet is produced by an injector with a needle length L over D ratio equal to 10. This ratio generates jets for which the velocity profile may play a preponderant role in the atomization processes depending on the nature of the liquid (see further details later). Microdisplacements allow block displacements of the injector and the needle in any direction. A laser sheet is produced by a He-Ne circular Gaussian beam traveling through an optical system [15]. The collected intensity in the forward direction, using a method of ombroscopy, is linearly related to the jet diameter [16]. The laser sheet thickness (30 μm) associated with a sufficiently high sampling rate (at least $100f_R$ where f_R is the Rayleigh frequency of the jet) then allows accurate measurements of the time evolution of the jet diameter. A sketch of the experimental setup is displayed in Fig. 1. Time series are recorded for successive locations along the jet axis, from the needle to the breakup in droplets, in 0.25- or 0.50-mm steps, depending on the distance between the needle exit and the length L_{BU}, where the average breakup occurs.

Two kinds of liquid-gas jets are considered here. In the first type, the liquid is pure water, while in the second it is a water-glycerol mixture (70% in weight of glycerol). For both types, the flow rate V is set to three different values reported in Table I with the corresponding breakup length values and Rayleigh frequencies. Pictures of the jet for the six regimes

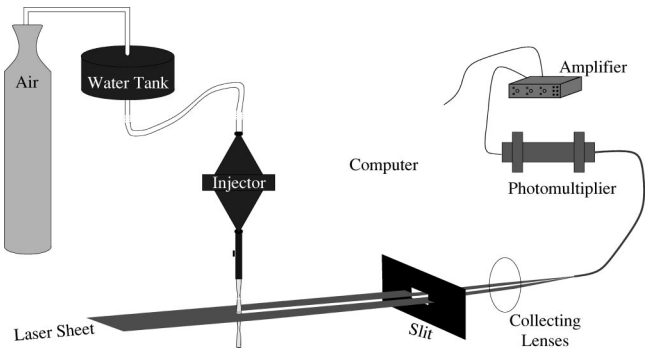

FIG. 1. Experimental setup for the liquid-gas jet investigation by ombroscopy.

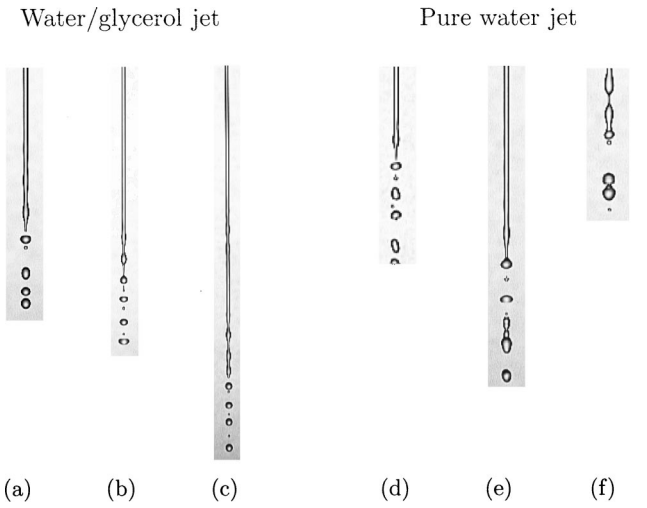

FIG. 2. Photos of free jets for the six different working conditions investigated here. (a) $V=1.28\,\mathrm{m\,s^{-1}}$, (b) $V=1.65\,\mathrm{m\,s^{-1}}$, (c) $V=2.15\,\mathrm{m\,s^{-1}}$, (d) $V=1.29\,\mathrm{m\,s^{-1}}$, (e) $V=1.66\,\mathrm{m\,s^{-1}}$, (f) $V=2.15\,\mathrm{m\,s^{-1}}$.

are displayed in Fig. 2. As observed on these six pictures, the breakup length L_{BU} depends on the flow rate V and on the nature of the liquid. Generically, the stability curve that represents the function giving the breakup length L_{BU} versus the flow rate V looks like the one displayed in Fig. 3. On this curve, a critical velocity V_C separates two types of dynamical behaviors. For the lower velocities, the breakup length increases with the flow rate. After the critical point located at V_C, the curve slope is negative. For a flow rate greater than V_C, the perturbations are initiated by the action of the velocity profile at the exit of the needle.

The three cases with the water-glycerol mixture and the first case with pure water are located on the increasing branch of the stability curve. Their dynamics are quite well-described by the linear Rayleigh theory. For $V=V_c=1.66\,\mathrm{ms^{-1}}$ with pure water [Fig. 2(e)], the working point is located at the critical point of the stability curve (Fig. 3) and, consequently, the Rayleigh frequency may be weakly significant. The last case [Fig. 2(f)] is clearly located on the decreasing branch of the stability curve.

B. Topological analysis

It has been demonstrated that working conditions are associated with two types of break-up mechanism related to the action of the velocity profile on the jet instability [17]. We will focus our attention on the water jet with a mean velocity $V=1.29\,\mathrm{m\,s^{-1}}$ that presents the same dynamics as the four others of the same class. The second class is only represented by the water jet at $V=2.15\,\mathrm{m\,s^{-1}}$. These two classes have been shown to be governed by different dynamics because the initial perturbation amplitudes are different [17]. The dynamics of these jets are now investigated by analyzing the time evolution of the jet diameter dynamics with tools borrowed from the nonlinear dynamical systems theory. An example of such analysis is displayed in Fig. 4 for an excited water jet with $V=0.81\,\mathrm{m\,s^{-1}}$ for which the dynamical structure is clearer than for free water jets [16]. The needle is characterized by a ratio L/D equal to 200 with an internal diameter $D=600\,\mu\mathrm{m}$. The needle length then allows a periodic excitation to be applied by a loudspeaker applied to the needle and connected to a frequency generator.

From the time evolution of the jet diameter [Fig. 4(a)], a phase portrait is reconstructed with the delay coordinates

$$X(t)=U(t),\qquad Y(t)=U(t+\tau). \tag{1}$$

The time delay τ is chosen to be equal to $1/(9F_E)$, where F_E is the excitation frequency. The organization of the trajectory in the phase portrait can be studied precisely with the first-return map [Fig. 4(c)]. For the excited jet, the first-return map presents an annular structure revealing that the dynam-

TABLE I. Physical properties of the six working conditions of liquid jet under study. Note that the Rayleigh frequency corresponding to the water jets with a flow rate equal to $1.66\,\mathrm{m\,s^{-1}}$ is only given as an indication and has no real physical meaning because this working point is not associated with conditions satisfying the Rayleigh theory. f_0 is the fundamental frequency computed from the experimental data. The Reynolds number is also reported.

	Water-glycerol			Pure water		
$V\,(\mathrm{ms^{-1}})$	1.28	1.65	2.15	1.29	1.66	2.15
$L_{BU}\,(\mathrm{mm})$	45.7	59.3	74.6	37.2	47.9	33.6
$f_R\,(\mathrm{Hz})$	473	610	795	477	614	
$f_0\,(\mathrm{Hz})$	440	640	840	540	580	650
Reynolds num.	17	49	64	773	994	1288

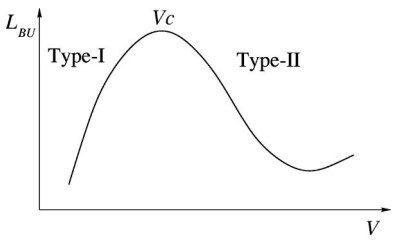

FIG. 3. The stability curve for liquid-gas jet. The increasing branch ($V<V_C$) corresponds to jet dynamics, well-described by the Rayleigh theory, while the decreasing branch ($V>V_C$) is here associated with atomization processes involving the effect of the velocity profile not taken into account by the linear theories. The three working points for the water-glycerol mixture and the first one for the pure water are located on the increasing branch.

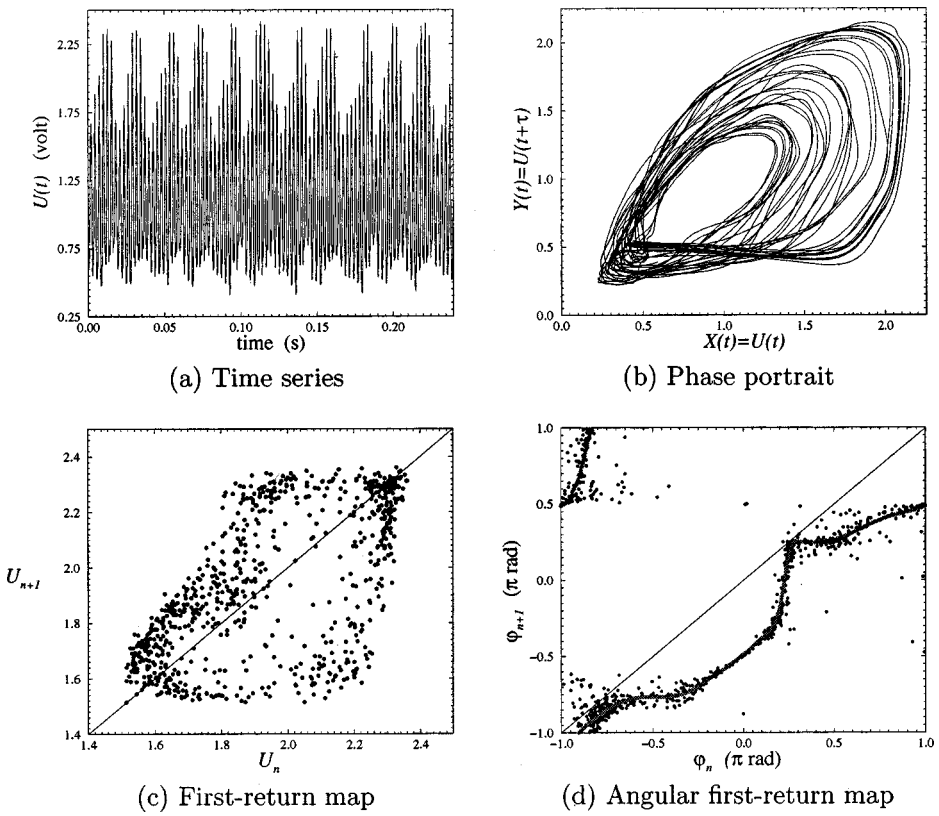

FIG. 4. The analysis is illustrated for $d=15.50$ mm, i.e., slightly before the breakup of an excited pure water jet. From the phase portrait (b) reconstructed from a time series (a) by using the delay coordinates, a first-return map to a Poincaré section is computed (c). This first-return map has an annular structure allowing one to define a phase angle φ to study the dynamics. The first-return map on φ (d) is nearly tangent to the bisecting line at two points. A piecewise regression of this angular map computed by using a singular value decomposition (SVD) technique is superimposed (gray curve).

ics is mainly deterministic and is based on a two-frequency torus. In order to investigate this type of annular structure, a phase angle φ in polar coordinates is defined, corresponding to the angle between a given position vector and a reference vector defining the phase origin. A first-return map on the phase angle φ is then computed [Fig. 4(d)].

The points of the angular first-return map are confined to a curve that may be approximated by an interpolation Singular Valve Decomposition (SVD) algorithm. This map is twice nearly tangent to the first bissecting line on the interval $[-\pi; \pi]$. This particularity characterizes the presence of intermittent mechanisms on the phase angle involving ''turbulent phases'' where the dynamics is irregular, fast and strong and ''laminar phases'' in regions close to the tangencies, during which the dynamics is nearly periodic and slow. This description characterizes a *phase intermittency.*

In the case of the free jets, and for the working conditions located on the first increasing branch of the stability curve, the points of the angular first-return map [Fig. 5(d)] are essentially located around the curve approximated from the measurement on the excited water jet. The configuration of the angular first-return map is still recognizable even though the points spread out from the estimated curve. This means that the dynamics is mainly governed by a phase intermittency as exhibited on the excited water jet. This dynamical behavior is thus deterministic. In contrast, when the working conditions correspond to a point beyond the critical velocity, the points of the first-return map are not confined on any structure (Fig. 6) and visit all the possible positions. One may note that nonvisited regions on this angular first-return map are due to a property of the phase angle and are not related to the jet dynamics [16]. Consequently, the dynamics could be associated with stochastic processes since no structure may be observed. This feature confirms the great differences between the two kinds of atomization regimes depending on the working conditions. A deterministic dynamics characterized by a phase intermittency is observed for all the jets located on the first increasing branch of the stability curve while a stochastic dynamics governs the atomization processes when the jets have a mean velocity greater than the critical velocity for first regime jets only. The distinction between these deterministic and stochastic dynamics will be confirmed by means of symbolic sequence statistics as discussed in the next section.

III. SYMBOLIC SEQUENCE STATISTICS

A. Theoretical background

An aperiodic behavior may be generated by a simple map such as the logistic map

$$x_{n+1}=\mu x_n(1-x_n). \tag{2}$$

It has been shown that the behavior generated by such a map may be conveniently analyzed by using symbolic dynamics [18]. When the behavior settles down onto a chaotic attractor, it may be partitioned by using a topological criterion. Such a partition divides the phase space into q disjoint sets, each of which is labeled with a symbol. Consequently, the time evolution of the dynamical system is translated into a sequence of symbols labeling the partition elements visited by an orbit. In the case where the logistic map is considered, the partition is given by the critical point C that separates the two monotonic branches making up the map (Fig. 7). q is therefore equal to 2. Indeed, it may be shown that the increasing branch is an order-preserving branch while the de-

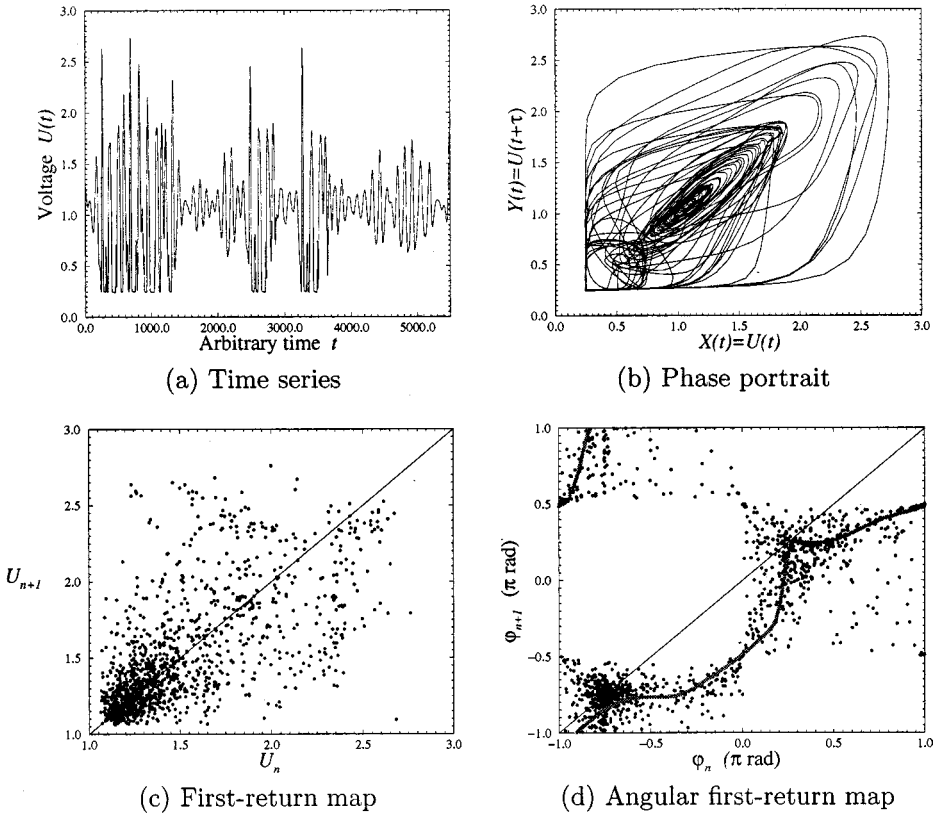

FIG. 5. The analysis is illustrated for a pure water jet with a flow rate $V=1.29\ \mathrm{m\,s^{-1}}$. The time evolution of the jet diameter (a) is recorded at a distance from the needle d equal to 33.75 mm, i.e., just before the breakup. From the phase portrait (b) reconstructed by using the delay coordinates, a first-return map to a Poincaré section (c) is computed. The angular first-return map on φ (d) is twice nearly tangent to the bissecting line. The angular first-return map is superimposed on the piecewise regression of the angular first-return map computed for the excited water jet.

creasing branch is an order-reversing branch [19]. Thus, a chaotic trajectory is described by a sequence $\{\sigma_n\}$ of symbols defined according to

$$\sigma_n=\begin{cases}0 & \text{if } x_n<x_C\\ 1 & \text{if } x_n>x_C,\end{cases} \tag{3}$$

where x_C is the coordinate of the critical point C. Such a map is said to be unimodal since a single critical point is involved.

When no partition can be given using a topological criterion, symbolic sequence statistical analysis may be used as introduced by Tang *et al.* [12,13]. In such a method, the first step is to choose the number q of the disjoint set into which the reconstructed state space is divided. We will see that this parameter may be important when the results are interpreted. Once this parameter is set, a numerical search is used to define partitions such that the individual occurrence of each symbol is equipropable with all others. Thus, a trajectory will visit equivalently each disjoint set defined by the statistical partition. For the sake of simplicity, the q symbols are chosen in the set $\Sigma_q=\{0,1,...,q-1\}$. Once the partition is defined, a trajectory is encoded as is usually done for any kind of symbolic dynamics.

The dynamics are investigated in a Poincaré section. The sequence of intersections between the trajectory and the Poincaré plane is converted into a symbol sequence by using a threshold function. The sequence of intersections $\{P_i\}_{i=1}^{N}$ is encoded into $\{\sigma_i\}$, where $\sigma_i\in\{0,1,...,q-1\}$ are used. It is defined according to our choice for equiprobable symbols. For a given time series of length N, the probabilities of various symbol sequences can now be estimated. Many levels of investigation may be used according to the length n of symbol sequences considered. At the first level, only the one-symbol sequences are considered and we thus have q probabilities characterizing the dynamics, namely $P_0,P_1,...,P_{q-1}$, where P_i is the probability of observing the symbol i. All P_i are obviously equal to $1/q$. When the two-symbol sequences are considered, q^2 probabilities describe the dynamics. For instance, P_{13} is the probability of observing the sequence ''13,'' and so on. At the nth level, q^n probabilities are used. The higher the level, the better the description of the dynamics. But to ensure that the statistics remain sufficiently well-defined, the choice of n is limited by

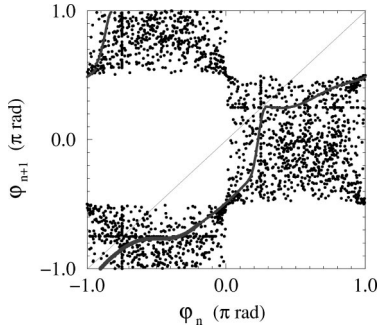

FIG. 6. Angular first-return map built on a phase angle φ defined on a basic first-return map for the velocity $V=2.19\ \mathrm{m\,s^{-1}}$ with a pure water jet. The time evolution for the jet diameter is recorded for $d=27.00$ mm, i.e., just before the breakup. The working conditions are located on the decreasing branch of the stability curve, i.e., correspond to a jet for which the action of the velocity profile at the needle exit is preponderant in the atomization processes. For comparison, an approximation performed in the case of an excited jet is represented on this figure by a gray curve.

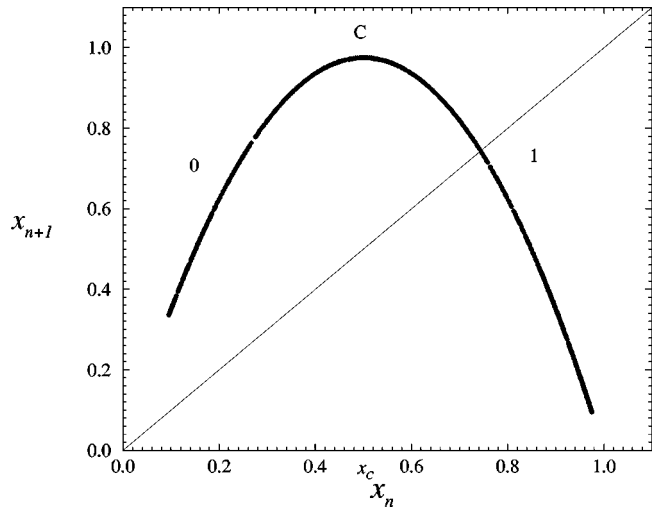

FIG. 7. Chaotic behavior generated by the logistic map ($\mu = 3.9$). The critical point is located at the maximum, i.e., $x_C = 0.5$ for any μ values.

the length N of the set of intersections $\{P_i\}$. With $N = 10\,000$, we limit the choice of n as follows:

q	2	3	4	5
n	6	4	3	3
q^n	64	81	64	125

i.e., $1/q^n \approx 1\%$.

A statistical analysis is only possible through investigating the different probabilities for sequences of a given length n occurring. The analysis may then provide a histogram giving such probabilities. In order to obtain the histograms, the different symbolic sequences are ordered as follows. The q^n possible sequences composed of n symbols chosen among q different symbols are indexed according to the natural order of the integer expressed in the q basis. For instance, in the case where binary symbolic dynamics is considered, the sequence 000 100 is associated with the index $i = 4$, which is the integer corresponding to the binary number 000100.

A first investigation with symbolic sequence statistical analysis is achieved in the case where the logistic map is iterated for four different values of the control parameter μ for which the kneading sequence [18], i.e., the symbolic sequence of the last created periodic orbit, is identified below:

μ	Kneading sequence
3.70	(1011 111)
3.90	(1001 010)
3.98	(1001 1)
3.9999	(1000 001)

The four different maps are displayed in Fig. 8. The critical point C is displayed as well as the point C_S defining the statistical partition involving the two symbols. One may observe that when the control parameter μ is increased, the point C_S tends toward the critical point C. When the symbolic dynamics is complete, i.e., all possible sequences built with the symbol set $\Sigma_q = \{0,1,...,q-1\}$ correspond to a periodic solution embedded within the attractor, the critical point C and the point C_S are located at approximately the same place. This means that the generating partition defined by the critical point C induces equiprobable symbols, too. By investigating the histograms computed for the four μ values, it is observed that different sequences appear when the control parameter is increased (Fig. 9) as expected from a rigorous description of the evolution of the periodic spectrum. Nevertheless, when $\mu = 3.9999$, a flat histogram is found, showing that all sequences of six symbols are equiprobable. Such a

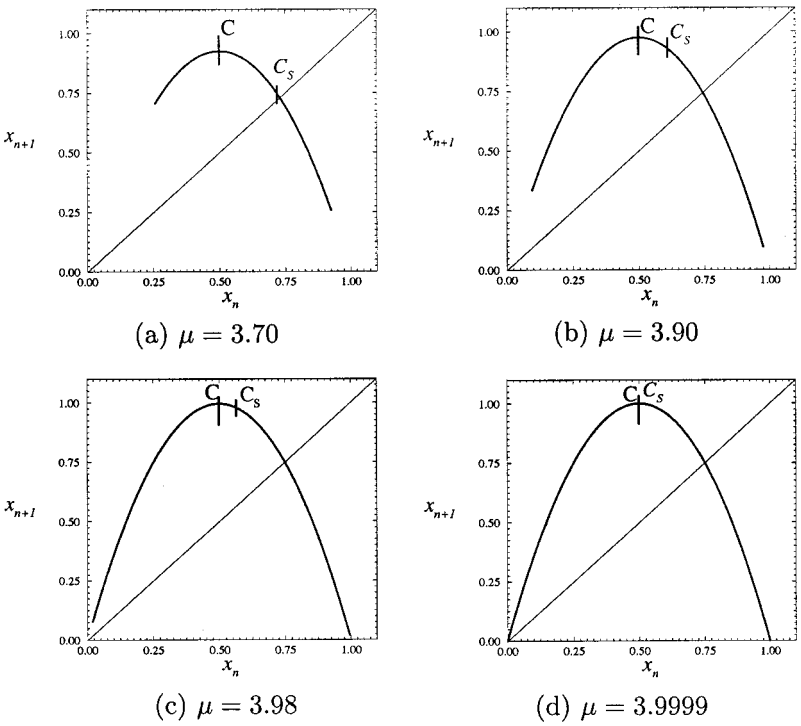

FIG. 8. Different configurations of the logistic map. The statistical partition defined by C_S tends to be equal to the generating partition, given by the critical point C, when the control parameter is increased. One may also note that the chaotic behavior is more fully developed, i.e., new sequences are authorized, when μ is increased.

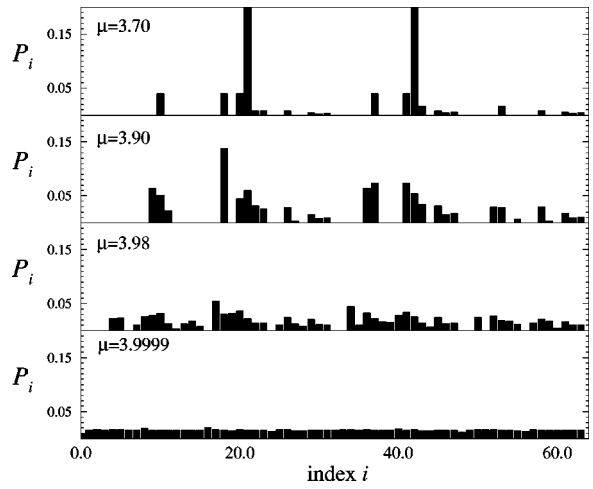

FIG. 9. Histogram giving the probability of realization of a sequence. The statistics are computed over 10 000 points ($q=2$,$n=6$).

flat histogram may be associated with white noise but not with a colored or autoregressive noise.

We would like to check whether this conjecture is general, i.e., if it remains true for any kind of map. A statistical analysis is therefore computed for different cases. The first one corresponds to the antisymmetric cubic map

$$x_{n+1}=\mu x_n^3+(1-\mu)x_n, \tag{4}$$

for $\mu=4.0$ for which three symbols are involved in the generating partition. The second case is provided by the quartic map

$$x_{n+1}=-\mu x_n^4+\mu x_n^2-1, \tag{5}$$

for which three critical points located at ± 0.5 and 0.0 separate four monotonic branches. The corresponding symbolic dynamics over the symbol set $\Sigma_4=\{0,1,2,3\}$ is complete for $\mu=8.0$. The histograms given by the symbolic sequence statistics [$(q=3, n=4)$ and $(q=4, n=3)$, for the cubic and the quartic maps, respectively] are both flat as displayed in Fig. 10. Again, a complete symbolic dynamics on Σ_q is associated with a flat histogram when symbol sequence statistics are performed with the number of symbols induced by the topological partition. Symbol sequence statistics are therefore a very useful tool to detect completeness of symbolic dynamics. Indeed, as we observe in the case of the logistic map (Fig. 9), a slight departure from the control parameter value for which the completeness is observed on the cubic and the quartic maps may be identified.

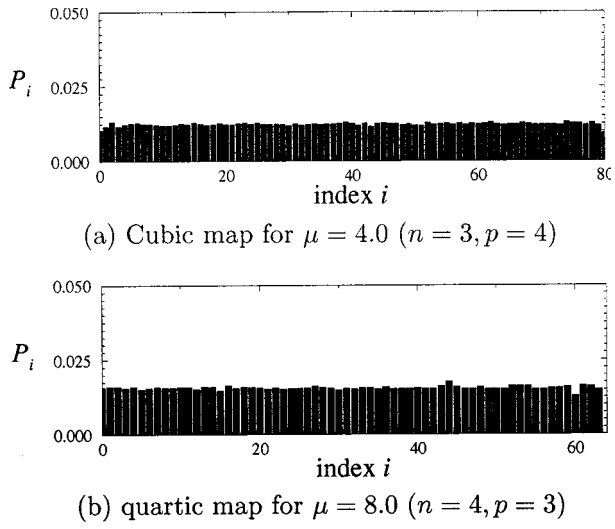

FIG. 10. Symbolic sequence statistics for two different maps with complete symbolic dynamics. As conjectured, the histograms are flat, i.e., all sequences of any length are equiprobable when the number of symbols for the statistics is equal to the number of disjoint sets induced by the generating partition.

This ability of the statistical analysis may greatly help in searching for control parameter values with complete symbolic dynamics. However, such flat histograms may also be associated with white noise. Thus, it may not be possible to distinguish such a stochastic behavior from deterministic dynamics characterized by complete symbolic dynamics. Indeed, faced with experimental data whose equations are unknown, an additional criterion is required to distinguish a deterministic behavior characterized by complete symbolic dynamics from white noise for which all sequences of any length are equiprobable too. The key is then to investigate the dynamics by varying the number of symbols q with which the trajectory is encoded.

In this way, the histogram is found to be flat only when the statistic partition corresponds to the topological partition, i.e., when the number of symbols q is equal to the number of disjoint sets defined by the generating partition. In other cases, some dominant sequences exist as exhibited in Fig. 11. A deterministic behavior characterized by complete symbolic dynamics may thus be distinguished from white noise, since in the latter case the histograms remain flat for every choice of q and n. When the dynamical behavior is like white noise, the histogram remains flat for any number of symbols used. Nevertheless, it should be mentioned that such a feature is not true for colored noise. Indeed, starting from a time series generated by the logistic map for $\mu=3.98$, we used a Fourier transform to randomize the phase. In this case, although the histogram is different from the one displayed in Fig. 9, it is not flat at all. Thus, when a histogram is found to be flat for any values of q, it may be stated that the dynamical behavior is white noise.

B. Analysis of free liquid-gas jets

We showed in the previous section that with statistical symbolic dynamics, white noise can be distinguished from other kinds of dynamics. Moreover, the number of the most probable sequences reveals the complexity of the dynamical regime. This technique is now applied to free liquid jets. In our cases, it will be shown that, depending on the working parameters, the underlying dynamics may be either deterministic, since it is associated with intermittencies, or white noise.

The procedure for constructing a histogram from an experimental time series is similar to the one used for the analysis of the logistic map, since it is applied to the first-return map computed from the reconstructed phase portrait, i.e., a discrete map.

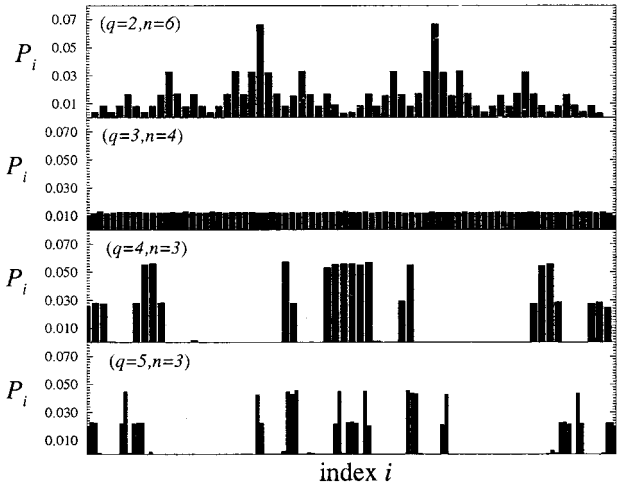

(a) Cubic map for $\mu = 4.0$

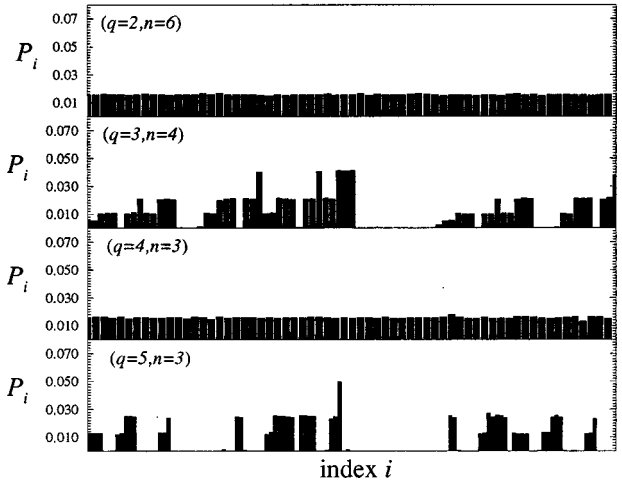

(b) quartic map for $\mu = 8.0$

FIG. 11. Different investigations for resolving the flatness of the histograms. The fact that a flat histogram is obtained for single values of the number of symbols q is a signature of deterministic dynamics characterized by complete symbolic dynamics. Such a behavior can therefore be distinguished from white noise for which the histograms remain flat independently of the values of q and n. In the case of the quatric map, a flat histogram is also obtained for $q = 2$ because the statistical partition then corresponds to one critical point of the topological partition. These two regions are thus associated with two symbols each. Since each symbol is equiprobable, both regions regions are equally visited.

Among the six different working points, it has already been established that one is governed by very different dynamical behavior from the others, i.e., the nonstructured angular first-return map observed for the case where the liquid is pure water with a flow rate equal to 2.15 $\mathrm{m\,s^{-1}}$ suggests that the dynamical behavior is stochastic. While phase intermittency has been identified for the five other working points, such a characteristic behavior is not observed for the pure water with $V = 2.15\,\mathrm{m\,s^{-1}}$. Histograms have been computed for this regime with $(q = 2, n = 6)$ and are displayed in Fig. 12. No sequence seems to be clearly dominant for this regime, at least up to the breakup located around 33.6 mm

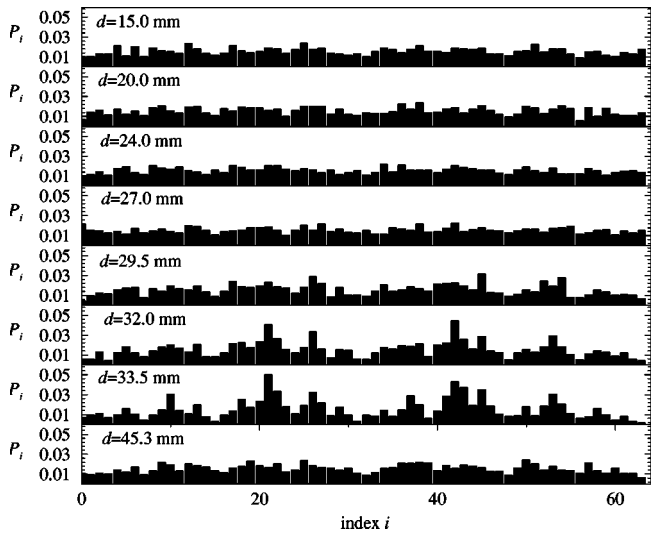

FIG. 12. Histograms for a free water jet with a flow rate equal to 2.15 $\mathrm{m\,s^{-1}}$. They have been computed for a few distances from the needle. Histograms are found to be mainly flat except near the breakup where a slight preponderance of a few sequences is observed.

from the needle. All sequences are essentially equiprobable as would be observed for white noise. Around the breakup ($d = 32.0$ mm and $d = 33.5$ mm), a few sequences may be distinguished from the others. They mainly correspond to sequences such as 010101 or 101010. The symbol ''1'' may be associated with oscillation that will become a droplet after the breakup. The symbol ''0'' corresponds to a small ligament that will become a satellite (tiny droplet) after the breakup. After the breakup, droplets and satellites may sometimes collapse together. A flat histogram is then recovered. The symbolic sequence statistical analysis confirms that the dynamical behavior associated with this regime corresponds to white noise because a flat histogram is observed for $d = 45.3$ mm (Fig. 12).

For the five other working points investigated here and before the breakup, particular sequences are clearly exhibited as soon as the oscillations of the diameter have a sufficient amplitude to be measured, i.e., approximately from a distance $d = 20$ mm from the needle (Fig. 13). About ten sequences may be significantly distinguished from a statistical point of view and read as

000 000	100 000
000 011	110 000
000 111	111 100
001 111	111 100
011 111	111 111

These sequences correspond to bursts associated with intermittent processes. Series with large amplitude oscillations are separated by low amplitude perturbations. Such dynamical behavior corresponds to a jet whose typical shape reconstructed from the jet diameter measurements is displayed in Fig. 14.

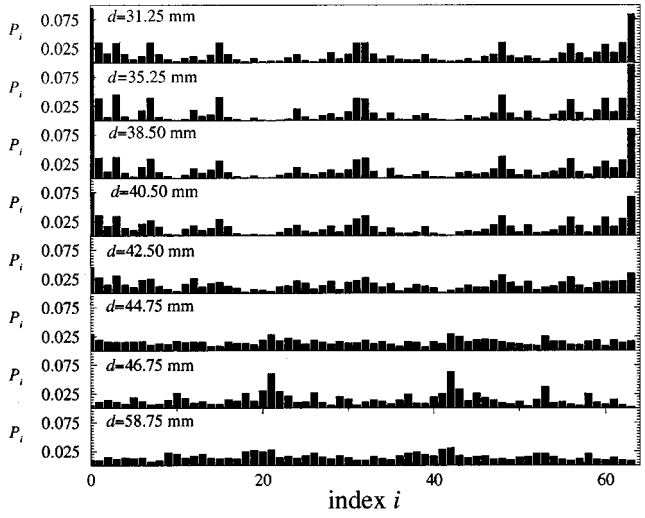

FIG. 13. Histograms for a free water jet with a flow rate equal to 1.66 m s^{-1}. They have been computed for a few distances from the needle. The histograms reveal deterministic dynamics as soon as the oscillation amplitudes are sufficiently large to be measured. Preponderant sequences progressively disappear to leave a flat histogram slightly before the breakup ($L_{BU}=47.90$ mm). As observed for the previous working point, sequences 010101 and 101010 are dominant slightly beyond the breakup. Such a feature is typical for the five remaining working points. ($q=2,n=6$).

These relevant sequences in the behavior tend to be less dominant in the dynamics when the distance from the needle is increased. Near $d=44.75$ mm, there is a transition region before the breakup ($L_{BU}=59.3$ mm) where the histogram is nearly flat and all sequences are equiprobable. In order to check whether the dynamics are white noise or not, we computed histograms for different numbers of symbols (Fig. 15). When the number of symbols is set at 3 or 4, the histogram

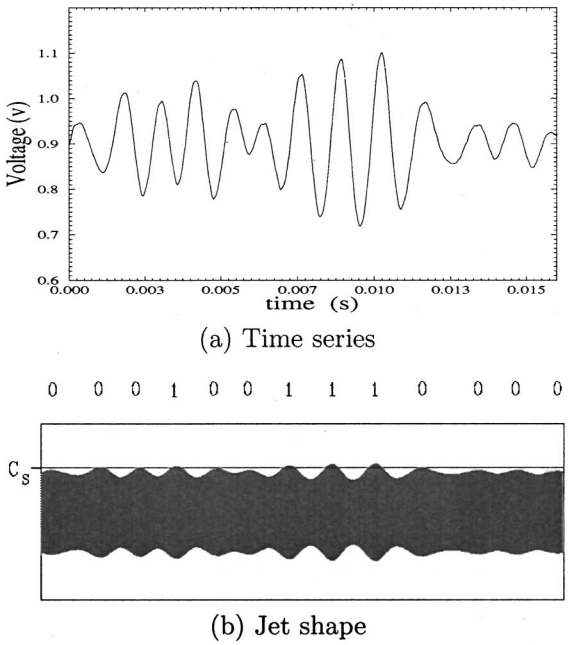

FIG. 14. Reconstruction of the jet shape from the diameter measurements for a distance from the needle $d=42.50$ nm. The symbols defined by the statistical symbolic dynamics are also reported.

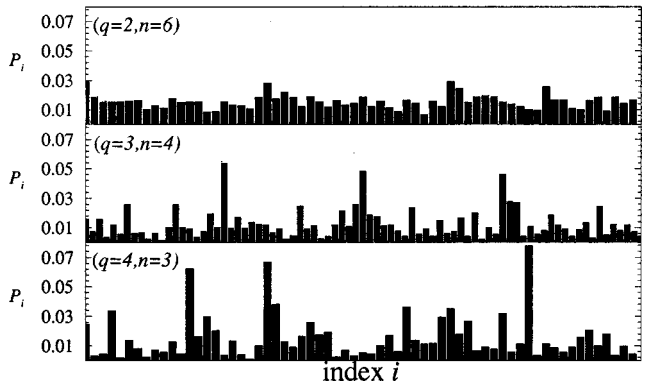

FIG. 15. Histograms computed slightly before the breakup ($d=44.75$ mm) for a water jet with a flow rate equal to 1.66 m s^{-1}. Peaks appear when the number of symbols is increased. The underlying dynamics are therefore deterministic as suggested by the angular first-return map.

does not remain flat and few peaks are observed. We showed in Sec. II B that such a feature is characteristic of a complete symbolic dynamics. Consequently, it seems that the atomization processes at the breakup are governed by a complete binary symbolic dynamics. We have at least ensured that the atomization processes near the breakup are not white noise. This is quite an important result since it suggests that atomization processes could be controlled.

After the breakup, we recover the resonance observed for the stochastic regime. Indeed, sequences 010101 and 101010 mainly dominate the dynamics at this stage. They correspond to a succession of single droplets each with one satellite. It seems that such behavior is actually characteristic of the atomization processes. If the investigation is pursued far from the breakup ($d=58.75$ mm), it is observed that the histogram is nearly flat. Other computations done by increasing the number of symbols do not induce any significant change in the shape of the histogram (Fig. 16), as any droplet and satellite couple has relaxed into a larger droplet whose size is nearly constant. Thus, only small fluctuations in the size of the diameter are measured. Nearly flat histograms reveal that these low amplitude fluctuations are governed by white noise.

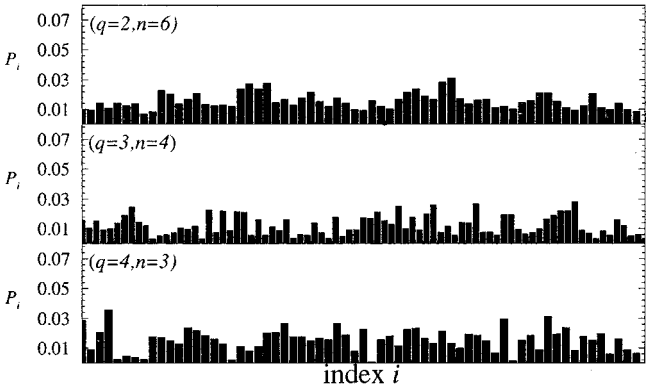

FIG. 16. Histograms computed far from the breakup ($d=58.75$ mm) for a water jet with a flow rate equal to 1.66 m s^{-1}. Increasing the number of symbols does not induce the presence of obvious peaks. Diameter oscillations could be therefore identified as white noise.

IV. CONCLUSION

Different working points for free liquid jets have been investigated by using a symbol sequence statistics. This interesting technique was first used on simple maps to highlight the kind of knowledge that may be obtained about dynamical behavior. It has been observed that when chaotic behavior becomes more developed, the number of relevant sequences increases too. An interesting feature has been observed in the case where the dynamical behavior studied is characterized by a complete symbolic dynamics for which all sequences are equiprobable. In order to distinguish such behavior from white noise for which all sequences are equiprobable too, it is sufficient to increase the number of symbols involved in the symbol sequence statistics, dominant sequences being recovered in the case of a deterministic behavior characterized by a complete symbolic dynamics.

Such a technique was thereafter used to analyze the dynamics underlying free liquid-gas jets. Among the six working points investigated here, one is found to be white noise. It corresponds to a working point for which the instabilities are governed by the velocity profile and no longer by the capillary instabilities as observed for the five other working points although the capillary instabilities still govern the perturbation growth. In the latter cases, atomization processes are clearly governed by a deterministic dynamics characterized by intermittencies as suggested by the angular first-return map and the symbolic sequence analysis. Such atomization processes can therefore be controlled by an external constraint to be defined. At the breakup, the behavior could be described in terms of a complete binary symbolic dynamics. It could therefore be possible to modelize the time evolution of the diameter by a quite simple map that remains to be discovered.

ACKNOWLEDGMENTS

We wish to thank gratefully Christophe Dumouchel for helpful discussions and encouragements. We wish also to thank Dilys Moscato for helping us to improve the English of this paper.

[1] L. Rayleigh, Proc. London Math. Soc. **10**, 4 (1878).
[2] C. Weber, Z. Angew. Math. Mech. **11**, 136 (1931).
[3] S. Leroux, C. Dumouchel, and M. Ledoux, Atomization Sprays **6**, 623 (1996).
[4] G. Broze and F. Hussain, J. Fluid Mech. **311**, 37 (1996).
[5] A. Brandstäter and H. L. Swinney, Phys. Rev. A **35**, 2207 (1987).
[6] A. Libchaber and J. Maurer, J. Phys. (France) Lett. **41**, C3 (1980).
[7] P. Bergé, M. Dubois, P. Manneville, and Y. Pomeau, J. Phys. (France) Lett. **41**, L344 (1980).
[8] D. J. Olinger and K. R. Sreenivasan, Phys. Rev. Lett. **60**, 797 (1988).
[9] D. J. Olinger, Phys. Fluids A **5**, 1947 (1993).
[10] G. Vittori and P. Blondeaux, Phys. Fluids A **5**, 1866 (1993).
[11] F. N. Madden and T. Mullin, Phys. Fluids **7**, 2364 (1995).
[12] X. Z. Tang, E. R. Tracy, A. D. Boozer, A. de Brauw, and R. Brown, Phys. Rev. E **51**, 3871 (1995).
[13] X. Z. Tang, E. R. Tracy, and R. Brown, Physica D **102**, 253 (1997).
[14] C. S. Daw, M. B. Kennel, C. E. A. Finney, and F. T. Connelly, Phys. Rev. E **57**, 2811 (1998).
[15] J. Godelle, C. Letellier, and G. Gouesbet, in *Proceedings of the Third International Conference on Multiphase Flows '98, Lyon, France, 1998*, edited by J. Bataille and M. Lance, pp. 167–176. (Reprints available upon request to the authors.)
[16] J. Godelle, Ph.D. thesis, Université de Paris VII, 1999.
[17] J. Godelle, C. Letellier, and C. Dumouchel, in *Proceedings of the 8th International Conference on Liquid Atomization and Spray Systems, Pasadena, 2000*, edited by N. Chigier, pp. 106–112 (CD-rom available upon request to jat@ucicl.uci.edu).
[18] P. Collet and J. P. Eckmann, in *Iterated Maps on the Interval as Dynamical Systems*, edited by A. Jaffe and D. Ruelle (Birkhäuser, Boston, 1980).
[19] P. Bergé, Y. Pomeau, and Ch. Vidal, *L'Ordre dans le Chaos* (Hermann, Paris, 1984).